Drug-Induced Self-Assembly of Modified Albumins as Nano-theranostics for Tumor-Targeted Combination Therapy

Qian Chen,[†] Xin Wang,[‡] Chao Wang,[†] Liangzhu Feng,[†] Yonggang Li,[‡] and Zhuang Liu*[,†]

[†]Institute of Functional Nano & Soft Materials (FUNSOM), Collaborative Innovation Center of Suzhou Nano Science and Technology, the Jiangsu Key Laboratory for Carbon-Based Functional Materials & Devices, Soochow University, Suzhou, Jiangsu 215123, China and [‡]Department of Radiology, The First Affiliated Hospital of Soochow University, Suzhou, Jiangsu 215006, China

ABSTRACT Paclitaxel (PTX) can bind to human serum albumin (HSA) *via* hydrophobic interaction, forming Abraxane, which is a U.S. Food and Drug Administration (FDA) approved effective antitumor nanomedicine drug. Herein, the effective antitumor drug PTX is used to induce the self-assembly of HSA modified with either a photosensitizer chlorin e6 (Ce6), which at the same time serves as a chelating agent for Mn^{2+} to enable magnetic resonance imaging, or acyclic Arg-Gly-Asp (cRGDyK) peptide that targets $\alpha v\beta 3$-integrin overexpressed on tumor angiogenic endothelium. Two types of tumor-targeting theranostic nanoparticles are constructed, either by coassembly of both HSA-Ce6 and HSA-RGD simultaneously or by forming an HSA-Ce6@HSA-RGD core–shell structure, with the assistance of PTX-induced albumin aggregation. Such albumin-based nanoparticles on one hand could target $\alpha v\beta 3$-integrin, as evidenced by both *in vitro* and *in vivo* experiments, and on the other hand enable combined photodynamic/chemotherapy, which offers remarkably improved therapeutic efficacy to kill cancer in comparison to the respective monotherapies. Our work presents a new type of tumor-targeted multifunctional albumin-based nanoparticles by drug-induced self-assembly, which is a rather simple method without any sophisticated chemistry or materials engineering and is promising for multimodel imaging-guided combination therapy of cancer.

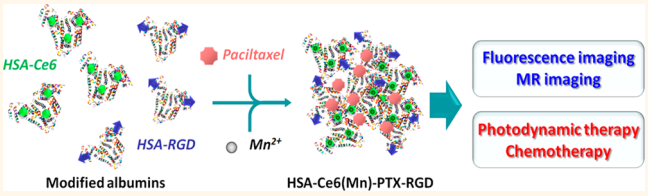

KEYWORDS: paclitaxel · human serum albumin · cancer targeting · self-assembly · combination therapy

In cancer treatment, chemotherapy has many drawbacks such as limited efficacy, severe toxic side effects, and the tendency to induce drug resistance.[1,2] To overcome such long-standing challenges, various tumor-targeted drug delivery systems have been developed to improve therapeutic efficiency and minimize toxic side effects.[3] On the other hand, the combination of various therapeutic strategies to treat cancer is another important and promising strategy to improve therapeutic efficiency and overcome drug resistance.[4−7] For example, chemotherapy can be combined with different therapies such as radiation therapy, gene therapy, magnetic hyperthermia therapy, and photothermal and photodynamic therapies, to achieve a synergistic antitumor therapeutic effect.[8−16]

However, simply mixing different therapeutic agents to treat cancer may not be able to achieve ideal therapeutic outcomes, partly because of their different pharmacokinetic profiles and inconsistent tumor uptake.[17] Recently, many drug-delivery systems (DDSs) based on various functional nanoparticles have been widely explored for applications in cancer combination therapy.[18−24] However, many of the currently explored DDSs may not be fully biocompatible, especially inorganic ones. Moreover, tedious chemical synthesis procedures or complicated materials engineering is often required to develop DDSs with highly integrated functionalities. Thus, designing and constructing completely biocompatible and biodegradable DDSs that can smartly incorporate different therapeutic and diagnostic functions as well as target molecules *via* simple and reliable approaches for combination therapy of cancer is of great importance.

Human serum albumin (HSA), a major component of serum proteins, has attracted

* Address correspondence to zliu@suda.edu.cn.

Received for review January 28, 2015 and accepted May 7, 2015.

Published online May 07, 2015
10.1021/acsnano.5b00640

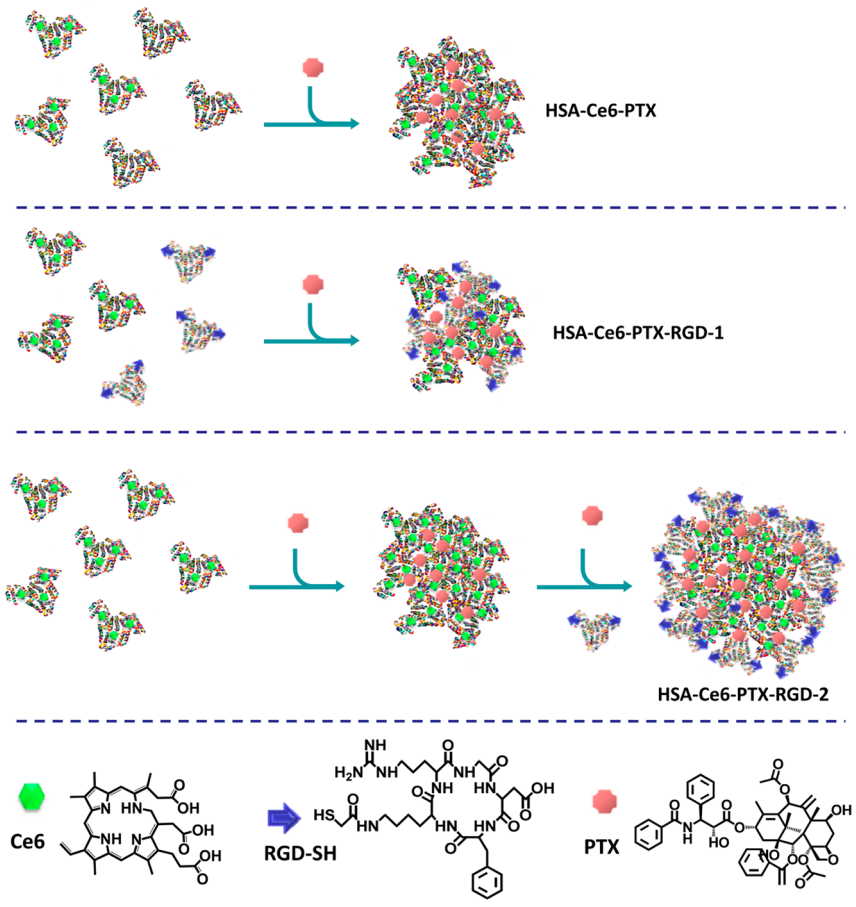

Figure 1. Schematic illustration showing the preparation of different formulations of albumin-based nanoparticles by drug-induced protein self-assembly.

wide interest as a natural drug carrier because of its inherent biocompatibility, abundance, and versatile roles in drug delivery.[25−36] Paclitaxel (PTX), an extensively used effective chemotherapeutical drug, is able to bind to HSA, forming drug-loaded protein nanoparticles with a trade name of Abraxane, which is an extremely successful example in nanomedicine for clinical cancer treatment.[37,38] In this work, we further report a simple method to construct albumin-based theranostic nanoplatforms *via* drug-induced protein assembly to realize tumor-targeted cancer treatment with combined photodynamic/chemotherapy. In our design, HSA is premodified with either chlorin e6 (Ce6), a photosensitizing agent, or cyclic Arg-Gly-Asp (cRGDyK) peptide, which targets $\alpha v\beta 3$-integrin upregulated on tumor vasculature endothelium and many types of tumor cells.[39−41] Tumor-targeted nanodrugs with the capabilities of multimodal imaging and combination therapy are then constructed *via* two strategies: (1) co-assembly of HSA-Ce6 and HSA-RGD upon addition of PTX (HSA-Ce6-PTX-RGD-1) or (2) mixing HSA-Ce6 with PTX first to form HSA-Ce6-PTX core nanoparticles, onto which HSA-RGD is assembled in the presence of additional PTX (HSA-Ce6-PTX-RGD-2) (Figure 1). Both types of nanoparticles are able to target $\alpha v\beta 3$-integrin-positive tumor cells *in vitro*. Obvious synergistic cancer cell killing is then observed using both nanoparticles under light irradiation, partly due to the accelerated endosomal escape of drugs as the result of photodynamic effect induced disruption of endosomes/lysosomes. Labeled with Mn^{2+} (by forming a chelate with Ce6), these nanoparticles could be tracked by dual modal magnetic resonance (MR) and fluorescence imaging, which reveal efficient tumor targeting of both formulations of nanodrugs. Tumor-targeted combination therapy is then successfully demonstrated *in vivo*, achieving outstanding therapeutic efficacy to kill tumors in animal experiments. Therefore, this work presents a simple approach to fabricate biocompatible multifunctional albumin-based theranostic agents with great potential for tumor-targeted combination therapy.

RESULTS AND DISCUSSION

In our work, HSA was first premodified with either Ce6 or RGD peptide. Ce6, a clinically used photodynamic agent, was conjugated to HAS *via* the formation of an amide bond. HSA-Ce6 with the optimized molar radio of HSA:Ce6 = 1:3 was chosen in our experiments (Supporting Figure S1). Meanwhile, thiolated

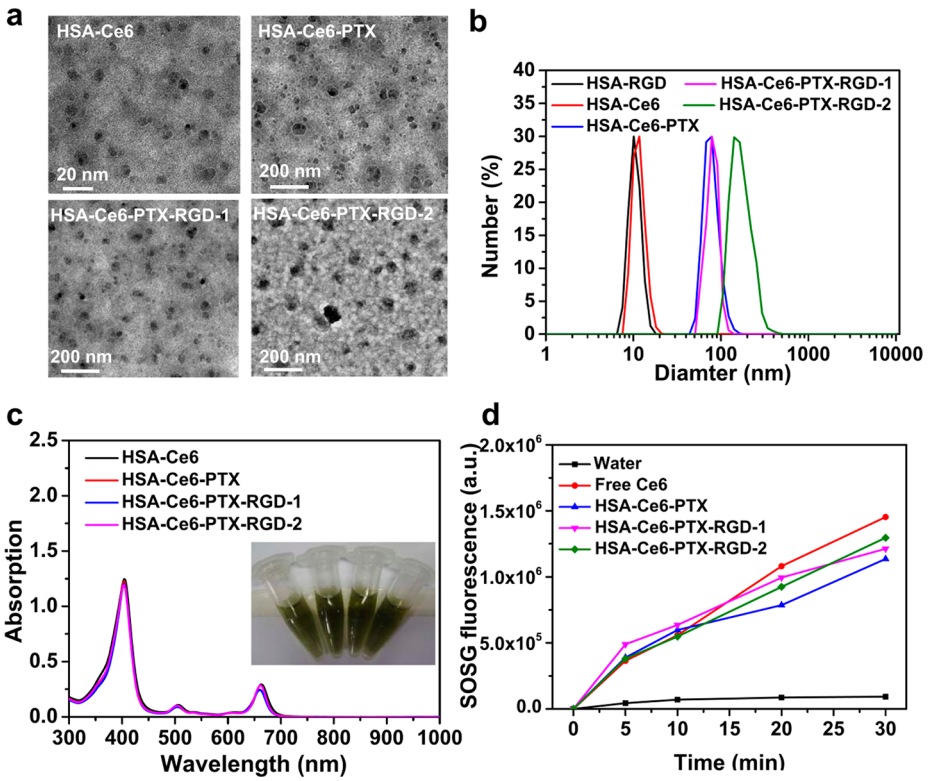

Figure 2. Characterization of albumin-based nanoparticles. (a) TEM images of HSA-Ce6, HSA-Ce6-PTX, HSA-Ce6-PTX-RGD-1, and HSA-Ce6-PTX-RGD-2. (b) Hydrodynamic diameters of HSA-RGD, HSA-Ce6, HSA-Ce6-PTX, HSA-Ce6-PTX-RGD-1, and HSA-Ce6-PTX-RGD-2 measured by DLS. It was the PTX that induced the self-assembly of albumin proteins. (c) UV−vis−NIR spectra of HSA-Ce6, HSA-Ce6-PTX, HSA-Ce6-PTX-RGD-1, and HSA-Ce6-PTX-RGD-2. Inset: Photograph of HSA-Ce6, HSA-Ce6-PTX, HSA-Ce6-PTX-RGD-1, and HSA-Ce6-PTX-RGD-2 dispersed in PBS. (d) Generation of singlet oxygen by measuring the fluorescence intensity changes of SOSG. The increase of SOSG fluorescence was a result of SO generation.

RGD peptide, which specially binds $\alpha v\beta 3$-integrin, was linked to HSA with the help of a bifunctional malemide linker. PTX, a highly hydrophobic antitumor drug, was used to induce the self-assembly of HSA-Ce6 and HSA-RGD into nanoparticles due to hydrophobic interactions between drug molecules and the hydrophobic domain on HSA. Two formulations of tumor-targeting multifunctional albumin-based nanoparticles have been fabricated in our study (Figure 1). For the first formulation, HSA-Ce6-PTX-RGD-1 was obtained by simply mixing HSA-Ce6, HSA-RGD, and PTX simultaneously. For the second formulation, HSA-Ce6-PTX-RGD-2 was prepared by a two-step procedure: HSA-Ce6 was mixed with PTX to form HSA-Ce6/PTX core nanoparticles, into which HSA-RGD and additional PTX were added to allow coating of HSA-RGD/PTX on the core nanoparticles. For the control HSA-Ce6-PTX nanoparticles, a mixture of HSA-Ce6 and unmodified HSA (1:1 ratio) was added with PTX to ensure the same Ce6 and PTX loadings. The Ce6 and PTX content in these different formulations were measured to be almost identical, 2.7% for Ce6 and 6.3% for PTX, by UV−vis absorbance spectra and high-performance liquid chromatography (HPLC), respectively.

Transmission electron microscopy (TEM) imaging revealed that HSA-Ce6-PTX and HSA-Ce6-PTX-RGD-1 showed similar sizes at about 50 nm, which was larger than HSA-Ce6 due to the protein assembly induced by PTX. As expected, HSA-Ce6-PTX-RGD-2 with the HSA-Ce6/PTX core and HSA-RGD/PTX shell structure showed a much larger size at ~100 nm (Figure 2a). Such observation was in a good agreement with their hydrodynamic sizes measured by dynamic light scattering (DLS) (Figure 2b). Next, the UV−vis−NIR absorption and fluorescence spectra of different nanoparticles were recorded (Figure 2c). All these nanohybrids retained the characteristic absorption peaks of Ce6 (404 and 650 nm). The ability of free Ce6, HSA-Ce6-PTX, HSA-Ce6-PTX-RGD-1, and HSA-Ce6-PTX-RGD-2 to generate cytotoxic singlet oxygen (SO) was then measured by the singlet oxygen sensor green (SOSG).[42] The SO production efficiency of different types of nanoparticles, which could be determined by the recovered SOSG fluorescence, showed no appreciable difference (Figure 2d) at the same Ce6 concentration, allowing us to use these nanoparticles for photodynamic therapy for cancer.

We then tested the *in vitro* specific $\alpha v\beta 3$-integrin binding efficiency of those RGD-conjugated nanoparticles by confocal imaging and flow cytometry measurement. $\alpha v\beta 3$-integrin-overexpressing U87MG human primary glioblastoma cells were incubated with HSA-Ce6-PTX, HSA-Ce6-PTX-RGD-1, or HSA-Ce6-PTX-RGD-2 for 30 min at 4 °C and washed with phosphate

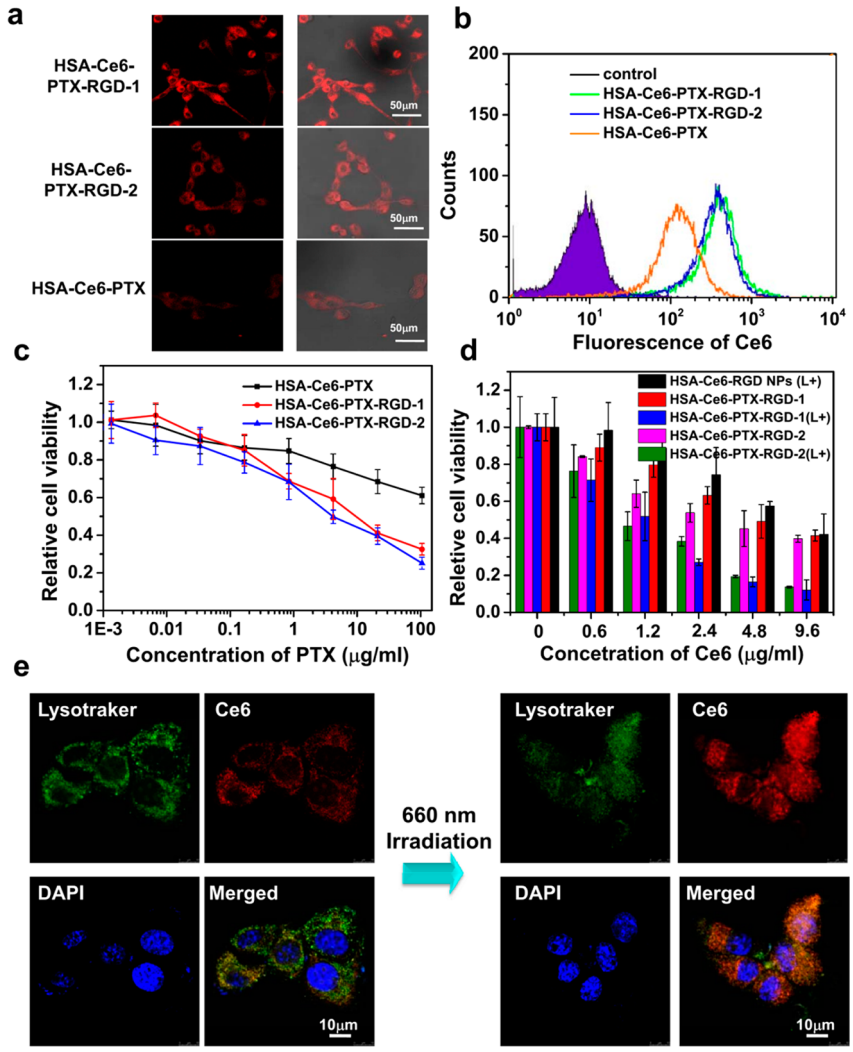

Figure 3. *In vitro* **cell culture experiments. (a and b) Confocal fluorescence images (a) and flow cytometry data (b) of U87MG cells incubated with HSA-Ce6-PTX-RGD-1, HSA-Ce6-PTX-RGD-2, and HSA-Ce6-PTX by recording Ce6 fluorescence. (c) Relative viabilities of U87MG cells after being treated with various concentrations of HSA-Ce6-PTX, HSA-Ce6-PTX-RGD-1, and HSA-Ce6-PTX-RGD-2. After incubation with nanoparticles for 30 min, the cells were washed and reincubated in free medium for 48 h before the MTT assay. (d) Relative viabilities of U87MG cells after incubation with HSA-Ce6-RGD, HSA-Ce6-PTX-RGD-1, and HSA-Ce6-PTX-RGD-2 with or without 660 nm light irradiation (2 mW/cm^2, 0.5 h). Those cells were then washed with PBS and reincubated in fresh medium for 24 h before the MTT assay. (e) Confocal fluorescence images of U87MG cells incubated with HSA-Ce6-PTX-RGD-1 for 2 h before and after 660 nm light irradiation (2 mW/cm^2, 1 h). Green, red, and blue colors represented LysoTracker-stained endosomes/lysosomes, Ce6 fluorescence, and DAPI-stained cell nuclei, respectively.**

buffer saline (PBS) to remove unbound nanoparticles. As expected, both confocal imaging and flow cytometry results revealed strong Ce6 fluorescence observed on U87MG cells incubated with HSA-Ce6-PTX-RGD-1 and HSA-Ce6-PTX-RGD-2, while cells treated with HSA-Ce6-PTX showed much weaker Ce6 fluorescence (Figure 3a,b). Therefore, both HSA-Ce6-PTX-RGD-1 and HSA-Ce6-PTX-RGD-2 showed effective molecular targeting capacity to specifically recognize $\alpha v\beta 3$-integrin overexpressed tumor cells.

Next, we tested the cell-killing efficacies of different PTX formulations *in vitro*. U87MG cells were incubated with free PTX (dissolved in a 1:1 (v/v) mixture of Cremophor EL and ethanol), HSA-PTX, and HSA-Ce6-PTX for 72 h. The relative cell viabilities were measured by the 3-(4,5-dimethylthiazol-2-yl)-2,5-diphenyltetrazolium bromide (MTT) assay. The cytotoxicities of the three PTX formulations were almost the same, proving that PTX after binding with HSA or HSA-Ce6 would retain its chemotherapeutic efficacy (Supporting Figure S2). The $\alpha v\beta 3$-integrin-targeted chemotherapy was then studied. U87MG cells were incubated with HSA-Ce6-PTX, HSA-Ce6-PTX-RGD-1, or HSA-Ce6-PTX-RGD-2 for 30 min and washed with PBS to remove excess nanoparticles. After further incubation in fresh cell medium for 48 h, the MTT assay was used to determine the relative cell viabilities. Compared to HSA-Ce6-PTX without RGD conjugation, HSA-Ce6-PTX-RGD-1 and HSA-Ce6-PTX-RGD-2 offered a much stronger cancer cell killing effect, owing to the specific $\alpha v\beta 3$-integrin recognition by RGD (Figure 3c).

Next, we evaluated the efficacy of targeted combined photodynamic /chemotherapy. U87MG cells

were incubated with various concentrations of HSA-Ce6-PTX-RGD-1 and HSA-Ce6-PTX-RGD-2 for 2 h. HSA-Ce6-RGD nanoparticles prepared by glutaraldehyde-induced cross-linking of HSA-Ce6 and HSA-RGD were used as the control for photodynamic therapy alone. After removal of free nanoparticles, cells were irradiated by 660 nm light at 2 mW/cm^2 for 30 min (optical dose = 3.6 J/cm^2). HSA coconjugated with both RGD and Ce6 was used as the control for only the photodynamic therapy. After incubation for another 24 h, the MTT assay was used to measure relative cell viabilities after different treatments. An obvious synergistic effect of the combined photodynamic/chemotherapy was observed (Figure 3d) for nanoparticle-treated cells after light exposure, showing superior cancer cell killing efficacies in comparison to photodynamic therapy alone (HSA-Ce6-RGD-treated cells with light irradiation) or chemotherapy alone (nanoparticle-treated cells without light exposure). The two formulations HSA-Ce6-PTX-RGD-1 and HSA-Ce6-PTX-RGD-2, despite their different structures and sizes, showed no obvious difference when they were used for *in vitro* cancer cell-targeted combination therapy.

To study the mechanism of the combined photodynamic and chemotherapy, U87MG cells were incubated with HSA-Ce6-PTX-RGD-1 (C_{Ce6} = 5 μM) for 2 h and washed with PBS to remove excess nanoparticles. Cells then were imaged by a confocal fluorescence microscope before and after being irradiated by 660 nm light for 30 min (Figure 3e). Before light irradiation, the fluorescence of Ce6 (red) was localized in endo/lysosomes, which were stained by LysoTracker (green), suggesting that nanoparticles were taken up by cells through endocytosis. In contrast, after the 660 nm light irradiation, remarkably reduced LysoTracker fluorescence and more diffused Ce6 fluorescence inside the cell cytoplasm were observed, implying the photodynamic effect induced degradation of endo/lysosomes and the subsequent endosomal escape of nanoparticles. On the basis of previous studies, it is known that photochemical reactions would induce endosomal opening to trigger cargo redistribution from endosomal vesicles to the cytoplasm or nucleus, improving the therapeutic efficiency of these cargos.[43] Such observation explains the improved therapeutic efficacy of the combined photodynamic/chemotherapy delivered by HSA-Ce6-PTX-RGD.

Next, we studied the tumor-targeting ability of RGD-conjugated albumin-based nanoparticles *in vivo*. Upon intravenous (iv) injection into mice, the three types of nanoparticles, HSA-Ce6-PTX, HSA-Ce6-PTX-RGD-1, and HSA-Ce6-PTX-RGD-2, exhibited similar blood circulation profiles as determined by measuring Ce6 fluorescence in the blood samples (Supporting Figure S3). Mice bearing subcutaneous $\alpha v\beta 3$-integrin-positive U87MG tumors were then iv injected with HSA-Ce6-PTX, HSA-Ce6-PTX-RGD-1, or HSA-Ce6-PTX-RGD-2 and imaged by a Maestro *ex vivo* imaging system at different time points. The fluorescence of Ce6 was distributed widely throughout the mouse body at early time points, likely due to the high concentration of nanoparticles in the blood. At later time points (*e.g.*, after 2 h and later), HSA-Ce6-PTX-RGD-1 and HSA-Ce6-PTX-RGD-2 showed obviously higher tumor accumulation in comparison to HSA-Ce6-PTX without RGD, suggesting the specific tumor binding ability of RGD-conjugated nanoparticles (Figure 4a,b). *Ex vivo* imaging at 24 h postinjection (pi) also revealed that Ce6 fluorescence intensities in the tumors of mice injected with HSA-Ce6-PTX-RGD-1 and HSA-Ce6-PTX-RGD-2 were ~2.42 and ~2.43 times higher than that of mice injected with HSA-Ce6-PTX, respectively (Figure 4c,d). Notably, the Ce6 signals in the tumors of mice injected with RGD-conjugated nanoparticles appeared to be higher than those in other organs including liver, spleen, and kidneys. The increased lung retention of RGD-conjugated nanoparticles might be attributed to the binding of RGD to $\alpha v\beta 6$-integrin, which is upregulated on proliferating epithelia in the lung.[44−46]

Fluorescence imaging with limited tissue penetration depth is only suitable for imaging of superficial tissues. MR imaging that allows whole-body imaging is an extensively used imaging modality in clinical diagnosis and prognosis of cancer. On the basis of previous studies, it is known that porphyrin and its derivatives can capture metal ions such as Mn^{2+} by forming stable chelates.[19,47] In this work, we used the porphyrin ring of Ce6 to chelate manganese-II (Mn^{2+}), which with five unpaired 3d electrons could offer T1 contrast in MR imaging and is known to be a metal ion with relatively low toxicity (Figure 5a).[48] By simply mixing HSA-Ce6 with Mn^{2+} and the subsequent removal of excess Mn^{2+}, HSA-Ce6(Mn) complex with a 1:1 Mn^{2+}:Ce6 ratio could be obtained as determined by inductively coupled plasma atomic emission spectroscopy (ICP-AES) measurement of Mn^{2+} (Supporting Figure S4). Under a clinical 3 T MR scanner, the T_1 relaxivity (r_1) of Ce6(Mn) was measured to be 5.41 mM^{-1} s^{-1}, while the r_1 values of HSA-Ce6(Mn), HSA-Ce6(Mn)-PTX, HSA-Ce6(Mn)-PTX-RGD-1, and HSA-Ce6(Mn)-PTX-RGD-2 were measured to be 14.6, 17.0, 17.5, and 24.5 mM^{-1} s^{-1}, respectively (Figure 5b and c). The integration of Mn^{2+} into nanoparticles would increase the local concentration of Mn^{2+} and lower the molecular tumbling rate of those Mn-containing complexes, thus resulting in increased r_1 values of those Mn^{2+}-containing nanoparticles.[49,50]

Taking advantage of the high r_1 values of the Mn^{2+}-labeled albumin-based nanoparticles, *in vivo* T_1-weighted MR imaging was carried out for U87MG tumor-bearing mice after iv injection of HSA-Ce6(Mn), HSA-Ce6(Mn)-PTX, HSA-Ce6(Mn)-PTX-RGD-1, and HSA-Ce6(Mn)-PTX-RGD-2 (Figure 5d). Consistent with the *in vivo* fluorescence imaging data, tumors on mice after injection of RGD-conjugated albumin-based nanoparticles showed a

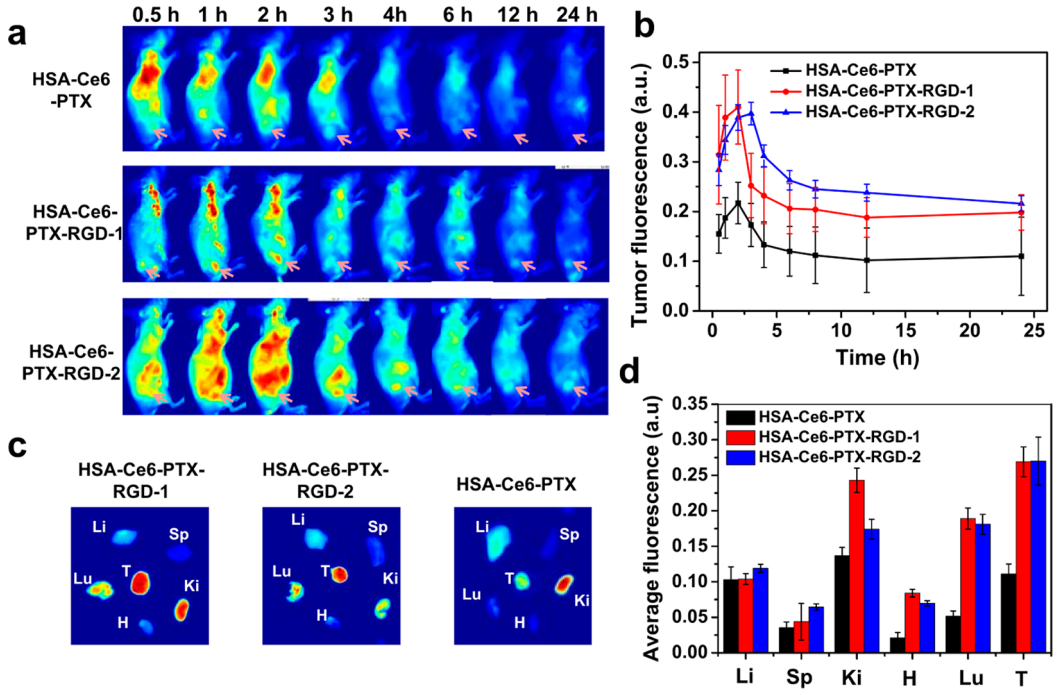

Figure 4. *In vivo* **and** *ex vivo* **fluorescence imaging. (a)** *In vivo* **fluorescence images of U87MG tumor-bearing nude mice taken at different time points post iv injection of HSA-Ce6-PTX, HSA-Ce6-PTX-RGD-1, and HSA-Ce6-PTX-RGD-2. (b) Relative fluorescence intensities of the tumors of different groups of mice at different time intervals based on** *in vivo* **fluorescence images shown in (a). (c)** *Ex vivo* **fluorescence images of major organs and tumor dissected from mice injected with HSA-Ce6-PTX, HSA-Ce6-PTX-RGD-1, and HSA-Ce6-PTX-RGD-2 at 24 h pi. Tu, Li, Sp, Ki, H, and Lu stand for tumor, liver, spleen, kidney, heart, and lung, respectively. (d) Semiquantitative relative biodistribution of HSA-Ce6-PTX, HSA-Ce6-PTX-RGD-1, and HSA-Ce6-PTX-RGD-2 in various organs as determined by the fluorescence intensities measured in (c).**

much stronger brightening effect compared to those injected with HSA-Ce6(Mn)-PTX (Figure 5d and e). No obvious increase of T1 signals was noted for tumors on mice injected with HSA-Ce6(Mn), likely due to its lower tumor retention and weaker T1 contrasting ability (Figure 5d,e). The biodistribution profiles of HSA-Ce6(Mn)-PTX, HSA-Ce6(Mn)-PTX-RGD-1, and HSA-Ce6(Mn)-PTX-RGD-2 were further determined by ICP-AES measurement of Mn levels in different organs (Supporting Figure S5). The tumor uptake of RGD-containing nanoparticles appeared to be ~2.5-fold of that of nontargeted nanoparticles. Therefore, both optical and MR imaging results as well as biodistribution data evidenced the efficient tumor targeting of our drug-loaded albumin-based nanoparticles with RGD conjugation, and the two formulations HSA-Ce6-PTX-RGD-1 and HSA-Ce6-PTX-RGD-2, although having different sizes, showed no significant difference in their tumor-targeting abilities.

Encouraged by the excellent combination therapeutic effect *in vitro* and efficient tumor targeting, we then carried out the tumor-targeted combined photodynamic/chemotherapy *in vivo*. On the basis of the aforementioned results, the two formulations of nanoparticles HSA-Ce6-PTX-RGD-1, formed by simultaneous coassembly of HSA-Ce6 and HSA-RGD, and HSA-Ce6-PTX-RGD-2, with a core/shell structure prepared by the two-step method, exhibited similar *in vitro* therapeutic efficacies and *in vivo* tumor-targeting capabilities. Considering the fact that HSA-Ce6-PTX-RGD-1 could be prepared *via* a simpler manner by just one step, HSA-Ce6-PTX-RGD-1 was chosen for our *in vivo* therapy experiment.

In our experiments, mice bearing subcutaneous $\alpha v\beta 3$-integrin-positive U87MG tumors were iv injected with PBS, HSA-Ce6-PTX, or HSA-Ce6-PTX-RGD-1 (doses: Ce6 5.4 mg/kg, PTX 12.6 mg/kg). Twelve hours after injection, the mice were irradiated by 660 nm light at a power density of 2 mW/cm^2 for 1 h (optical dose = 7.2 J/cm^2). Mice iv injected with the same dose of HSA-Ce6-PTX-RGD-1 but without light irradiation was used as the control. HSA-Ce6-RGD, with a much smaller sizes and distinctive pharmacokinetics, might not be a good control for *in vivo* photodynamic therapy alone and, thus, was not included in our experiments. After receiving various treatments, the tumor volumes were measured by a caliper every the other day. Tumors on mice treated with HSA-Ce6-PTX-RGD-1 but without light exposure in the absence of photodynamic effect showed a moderate growth inhibition effect only in the early days. The efficacy of HSA-Ce6-PTX plus 660 nm light irradiation also was not ideal due to the low tumor accumulation of these nanoparticles. Remarkably, the tumor growth on mice treated with HSA-Ce6-PTX-RGD-1 plus 660 nm light irradiation was almost completely inhibited (Figure 6a and Supporting Figure S6). Compared to mice in the three control groups, which

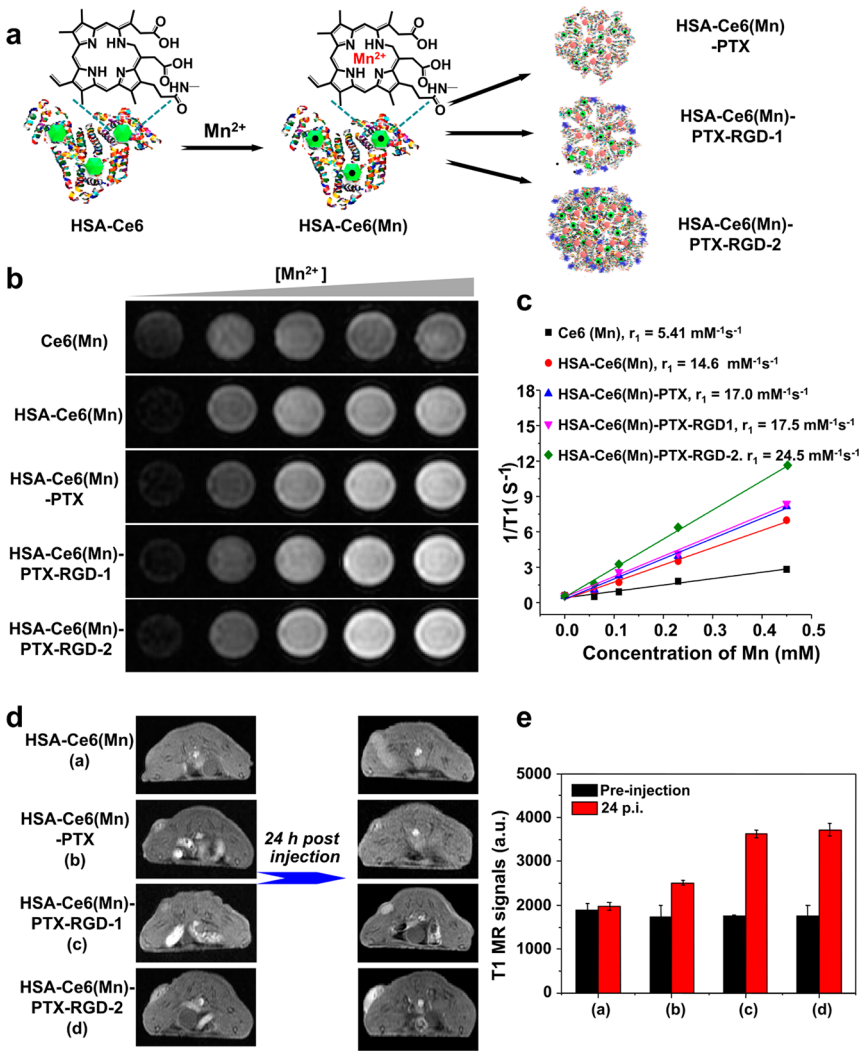

Figure 5. *In vivo* **MR imaging. (a) Scheme showing the preparation of the nanoparticles labeled with Mn^{2+}, which was chelated into the porphyrin structure of Ce6. (b and c) T_1-weighted MR images (b) and longitudinal relaxivity (r_1) (c) of Ce6(Mn), HSA-Ce6(Mn), HSA-Ce6(Mn)-PTX, HSA-Ce6(Mn)-PTX-RGD-1, and HSA-Ce6(Mn)-PTX- RGD-2 samples. (d) *In vivo* T_1-weighted MR images of mice taken before and 24 h postinjection of various Mn^{2+}-labeled agents. (e) Quantification of average T1-MR signals in the tumors by manually drawn region of interest before injection and 24 h postinjection based on images in (d). RGD conjugation could significantly enhance tumor homing of the albumin-based nanoparticles.**

showed average lifetimes of about 15−30 days, mice after tumor-targeted combination therapy (HSA-Ce6-PTX-RGD-1 + light) survived over 40 days without a single death (Figure 6b). Hematoxylin and eosin (H&E) staining of tumor slices, which were collected 2 days post-treatment, also confirmed that most cancer cells were completely destroyed in the tumor-targeted combination therapy group, while cells in the other control groups partly or largely retained their normal morphology (Figure 6c).

Our results have clearly demonstrated the high efficacy of tumor-targeted combination therapy of cancer using our albumin-based theranostic nanoparticles. Unlike many other nanoscale theranostic DDSs, which usually require sophisticated design and engineering, the albumin-based nanoagents presented in this work, which featured inherent biocompatibility, tumor-targeting ability, dual modal imaging functions, and the capability to deliver combined photodynamic/chemotherapy, are prepared by a rather simple method. Notably, the combination of photodynamic and chemotherapy delivered by our albumin-based theranostic nanoparticles not only is able to offer a synergistic therapeutic effect to kill a wide range of tumors but may also offer further advantages to overcome multidrug resistant (MDR) (Supporting Figure S7), a major challenge in current chemotherapy of cancer.

CONCLUSION

In conclusion, multifunctional albumin-based theranostic nanoparticles have been developed in this work for tumor-targeted drug delivery and dual-modal imaging-guided combination therapy of cancer. In our design, HSA premodified with either a photosensitizing molecule or a tumor-targeting peptide would self-assemble in the presence of a hydrophobic anticancer

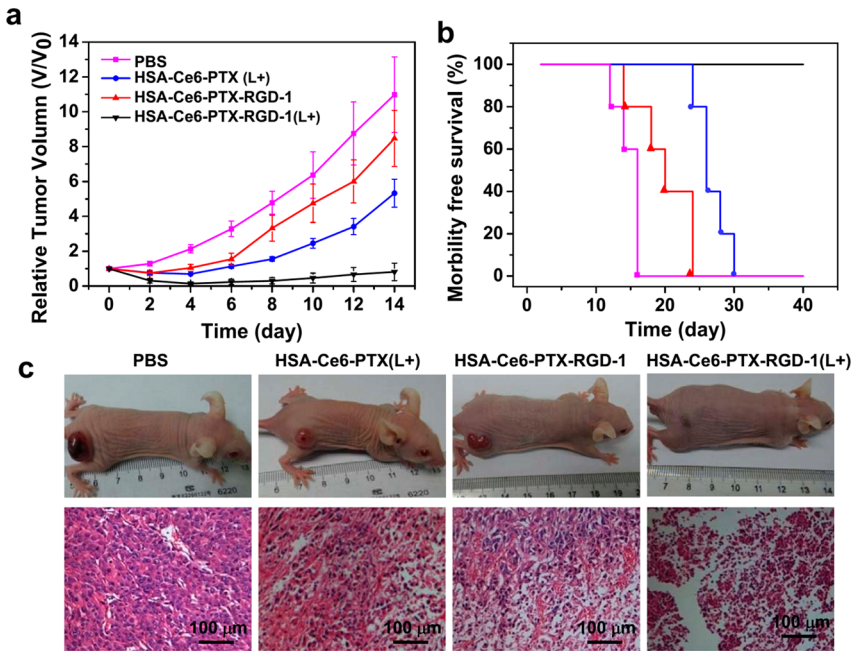

Figure 6. *In vivo* **tumor-targeted combination therapy. (a) Tumor growth curves of different groups of mice after various treatments indicated (5 mice per group): mice with PBS injection, mice injected with HSA-Ce6-PTX and exposed to 660 nm light irradiation (2 mW/cm^2, 1 h), mice injected with HSA-Ce6-PTX-RGD-1 without or with 660 nm light irradiation (2 mW/cm^2, 1 h). Error bars are based on standard errors of the mean (SEM). (b) Survival curves of mice bearing U87MG tumors after various treatments indicated in (a). (c) Representative photographs of mice from different groups taken at the 14th day (the upper row) and H&E-stained tumor slices collected from different groups of mice on the following day after various treatments (the bottom row).**

drug, PTX, to form tumor-targeting nanoparticles with multiple imaging and therapy functionalities. Two formulations of albumin-based nanoparticles were prepared by either a one-step method with coassembled HSA-Ce6 and HSA-RGD (HSA-Ce6-PTX-RGD-1) or a two-step method with the core (HSA-Ce6)/shell (HSA-RGD) structure. As a result of the photodynamic-effect-induced endosomal drug release, synergistic cancer killing is observed when HSA-Ce6-PTX-RGD (1 or 2)-treated cells are exposed to light irradiation. Upon systemic administration, efficient tumor targeting of RGD-conjugated nanoparticles is then realized as revealed by *in vivo* dual modal fluorescence/MR imaging. Utilizing the newly formulated HSA-Ce6-PTX-RGD-1 nanodrug, *in vivo* combination therapy is finally conducted, achieving an excellent tumor growth inhibition effect after iv injection of our tumor-targeted albumin-based nanomedicine and the combined photodynamic/chemotherapy. Our work presents a rather simple drug-induced self-assembly approach to construct protein-based theranostic nanoagents. With excellent biocompatibility and high therapeutic efficacy, our new tumor-targeted albumin-based nanodrugs may find great potential in the clinic for future imaging-guided cancer treatment. In addition, the drug-induced protein self-assembly strategy may be a useful concept to construct other types of protein-based multifunctional DDSs.

MATERIALS AND METHODS

Materials. Human serum albumin, 1-ethyl-3-(3-(dimethylamino)propyl)carbodimide (EDC), and *N*-hydroxysuccinimide (NHS) were obtained from Sigma-Aldrich. Paclitaxel and chlorin e6 were from J&K Chemical Co. Methanol (CH_3OH) and dimethyl sulfoxide (DMSO) were obtained from Sinopharm Chemical Reagent Co. 2-Iminothiolane (Traut's reagent) and sulfosuccinimidyl-4-(*N*-maleimidomethyl)cyclohexane-1-carboxylate (Sulfo-SMCC) were purchased from Pierce.

Synthesis and Optimization of HSA-Ce6-PTX-RGD Nanoparticles. Ce6 used during this experiment was predispersed in DMSO. To obtain HSA-Ce6, 0.1 mL of Ce6 (20 mg/mL, 1equiv), 0.064 mg of EDC (1 equiv), and 0.042 mg of NHS (1.1 equiv) were mixed in the dark for 0.5 h at room temperature. Then the activated Ce6-NHS was added into 1 mg of HSA dissolved in phosphate-buffered saline. The mixture was stirred overnight in the dark. HSA-Ce6 was obtained after centrifugation at 14 800 rpm for 5 min to remove possible aggregates and ultrafiltration by a centrifugal filter device (molecular weight cutoff (MWCO) = 10 kDa) three times to remove free Ce6.

For labeling with Mn^{2+}, manganese chloride ($MnCl_2$) was added to the solution containing HSA-Ce6 at a molar ratio of 2:1 ($MnCl_2$:Ce6). Excess $MnCl_2$ was removed using a centrifugal filter device (MWCO = 10 kDa). The concentrations of Ce6 and Mn^{2+} in the HSA-Ce6(Mn) complex were determined by UV−vis spectrum and ICP-AES, respectively.

HSA-RGD was synthesized in two steps. First, 1 mL of PBS containing 5 mg of HSA was mixed with 0.365 mg of Sulfo-SMCC (predissolved in 100 μL of DMSO). After 2 h of reaction, excess Sulfo-SMCC was removed using a centrifugal filter device (MWCO = 10 kDa) to purify SMCC-activated HSA. In the meantime, 0.3 mg of cRGDyK peptide was thiolated by reacting with Traut's reagent in PBS (pH 7.4) at a molar ratio of 1:0.9 for 2 h at 4 °C. Last, SMCC-activated HSA and RGD-SH were mixed in PBS

(pH 7.4) at a molar ratio of 1:10. After 24 h reaction at 4 °C, excess RGD was removed using the centrifugal filter device (MWCO = 10 kDa). The obtained HSA-RGD was stored at 4 °C until use.

HSA-Ce6-PTX-RGD-1 nanoparticles were prepared by PTX-induced self-assembly of albumin proteins. A 2 mg amount of HSA-Ce6 and 2 mg of HSA-RGD were mixed in PBS, into which 24 μL of PTX predissolved in methanol (20 mg/mL) was added. The obtained HSA-Ce6-PTX-RGD1 nanoparticles were purified by centrifugation at 14 800 rpm for 5 min to remove insoluble PTX and then ultrafiltration by a centrifugal filter device (MWCO = 10 kDa) three times to remove methanol. The control nontargeted HSA-Ce6-PTX nanoparticles were prepared by the same procedure except that 2 mg of plain HSA was used to replace HSA-RGD.

HSA-Ce6-PTX-RGD-2 nanoparticles were obtained through a two-step method. First, 12 μL of PTX(20 mg/mL) was added into 2 mg of HSA-Ce6 and stirred overnight. After removal of free PTX, 2 mg of HSA-RGD and an additional 12 μL of PTX were added to the mixture, which was then stirred overnight. The HSA-Ce6-PTX-RGD-2 solution was then purified by centrifugation (14 800 rpm for 10 min) to discard precipitates and ultrafiltration by a centrifugal filter device (MWCO = 10 kDa) three times. The obtained final products were stored in PBS at 4 °C.

PTX-free, HSA-Ce6, and HSA-Ce6-RGD nanoparticles were prepared for our control experiments by a glutaraldehyde-induced covalent albumin cross-linking method following a literature protocol.[51] Briefly, 10 mg of HSA-Ce6 or a mixture of 5 mg of HSA-Ce6 and 5 mg of HSA-RGD was dissolved in 2 mL of water, into which 2 mL of ethanol was dropwisely added under stirring at a rate of 0.5 mL/min. To induce cross-linking of proteins, 14 μL of 8% glutaraldehyde was added into the above solution, which was then stirred at room temperature for 12 h. HSA-Ce6 and HSA-Ce6-RGD nanoparticles were obtained after dialyzing these solutions against water to remove glutaraldehyde and ethanol and ultrafiltration by a centrifugal filter device (MWCO = 100 kDa) three times to remove free HSA.

Characterization. The morphology and structure of HSA-Ce6, HSA-Ce6-PTX, HSA-Ce6-PTX-RGD-1, and HSA-Ce6-PTX-RGD-2 after being stained by phosphotungstic acid (1 wt %) were characterized by TEM using a FEI Tecnai F20 transmission electron microscope. Fluorescence spectra of different samples were obtained on a FluoroMax 4 luminescence spectrometer (HORIBA JobinYvon). UV−vis−NIR absorbance spectra were recorded using a PerkinElmer Lambda 750 UV−vis−NIR spectrophotometer. The hydrodynamic diameters of the four complexes were determined by a Zetasizer Nano-ZS (Malvern Instruments, UK).

The encapsulation efficiency and release of PTX were determined by an HPLC (Agilent 1260) with a UV−vis detector at 227 nm. Acetonitrile was used as the mobile phase. The elution peak of PTX was found to be at 7.57 min. The loading ratio of PTX in these four complexes was almost identical (~6.3%).

The method for the singlet oxygen detection was based on the protocol reported previously.[52] In brief, 100 mg of SOSG (Molecular Probes, USA) was dissolved in 330 mL of methanol to obtain the stock solution of SOSG (0.5 mM). Then 10 μL of SOSG was added to 1990 μL of different sample solutions ([Ce6] = 1 μM). The different samples were irradiated by a lamp equipped with a 660 nm band-pass filter at a power density of 2 mW/cm^2. The fluorescence intensity of SOSG was measured under an excitation wavelength of 494 nm.

Cellular Experiments. Human glioblastoma U87MG cells were cultured in DMEM low-glucose medium containing 10% fetal bovine serum and 1% penicillin/streptomycin at 37 °C under 5% CO_2. For confocal imaging, U87MG cells ($\alpha v\beta 3$-integrin positive) were seeded in 35 mm culture dishes and treated with HSA-Ce6-PTX, HSA-Ce6-PTX-RGD-1, or HSA-Ce6-PTX-RGD-2 for 0.5 h at 4 °C. Such a low incubation temperature was able to reduce nonspecific binding and uptake of nanoparticles by cells. After washing with PBS (pH = 7.4) three times, the cells were labeled with 4,6-diamino-2-phenylindole (DAPI) and then imaged by a confocal fluorescence microscope (Leica SP5II).

To study the cell-killing efficacy of the different PTX formulations, U87MG cells were seeded into 96-well cell culture plates until adherent and then incubated with various concentrations of free PTX, HSA-PTX, and HSA-ICG-PTX for 72 h. The standard MTT (Sigma-Aldrich) assay was carried out to determine the cell viabilities relative to control untreated cells.

For targeted chemotherapy, U87MG cells were seeded into 96-well cell culture plates until adherent and then incubated with various concentrations of HSA-Ce6-PTX, HSA-Ce6-PTX-RGD-1, and HSA-Ce6-PTX-RGD-2. After 0.5 h of incubation at 4 °C, free materials were removed by washing twice with fresh culture medium. Afterward, the cells were reincubated in fresh medium at 37 °C for an additional 48 h before the MTT assay to determine the relative cell viabilities.

For combination therapy, U87MG cells were incubated with various concentrations of HSA-Ce6-PTX, HSA-Ce6-PTX-RGD-1, and HSA-Ce6-PTX-RGD-2. After 2 h of incubation, free materials were removed. Afterward, the samples were placed under 660 nm light irradiation at 2 mW/cm^2 for 0.5 h. After additional incubation for 24 h, the MTT assay was carried out to determine the cell viabilities relative to control untreated cells.

To study the mechanism of the combined photodynamic/chemotherapy, U87MG cells were incubated with HSA-Ce6-PTX-RGD-1 (C_{Ce6} = 5 μM) for 2 h and washed with PBS to remove excess nanoparticles. After the 660 nm light irradiation for 30 min, cells were incubated at 37 °C for another 2 h. Before confocal imaging, cells were labeled by LysoTracker (green) and DAPI to stain endosomes/lyosomes and nuclei, respectively.

Animal Model. Female nude mice were purchased from Nanjing Peng Sheng Biological Technology Co Ltd. and used under protocols approved by Soochow University Laboratory Animal Center. To develop the tumor model, 2 × 10^6 U87MG cells suspended in 50 μL of PBS were subcutaneously injected into the back of each mouse. The mice were used when tumor volumes reached about 50−60 mm^3.

***In Vivo* Imaging.** For *in vivo* imaging, 200 μL of HSA-Ce6-PTX, HSA-Ce6-PTX-RGD-1, and HSA-Ce6-PTX-RGD-2 with a 0.54 mg/mL Ce6 equivalent concentration was iv injected into each mouse (doses: Ce6 5.4 mg/kg, PTX 12.6 mg/kg). *In vivo* fluorescence imaging was conducted using a Maestro *in vivo* optical imaging system (Cambridge Research and Instrumentation, Inc.). To detect Ce6 fluorescence, we used red light with the center wavelength at 661 nm as the excitation light and collected emission spectra from 700 to 850 nm. Spectral unmixing was conducted by the Maestro software to remove the autofluorescence background. The mice were sacrificed 24 h after iv injection, with their major organs including the tumor, liver, heart, lung, spleen, and kidneys collected for *ex vivo* imaging. MR imaging was conducted by using a 3.0 T clinical MR scanner (GE Healthcare, USA) equipped with a small-animal imaging coil.

***In Vivo* Combination Therapy.** Nude mice bearing subcutaneous U87MG tumors (~60 mm^3) were divided into four groups (n = 5 per group): (a) iv injected with PBS; (b) iv injected with 200 μL of HSA-Ce6-PTX (20 mg/mL HSA, 0.54 mg/mL Ce6, 1.26 mg/mL PTX) and irradiated by 660 nm light (2 mW/cm^2, 1 h, 12 h after injection); (c) iv injected with 200 μL of HSA-Ce6-PTX-RGD-1 without light irradiation; (d) iv injected with 200 μL of HSA-Ce6-PTX-RGD-1 (20 mg/mL HSA, 0.54 mg/mL Ce6, 1.26 mg/mL PTX) and irradiated by 660 nm light (2 mW/cm^2, 1 h, 12 h after injection). The tumor sizes were recorded every 2 days for 2 weeks, with their lengths and widths measured by a digital caliper. The tumor volume was calculated according to the following formula: width^2 × length/2.

Conflict of Interest: The authors declare no competing financial interest.

Acknowledgment. This work was partially supported by the National Basic Research Programs of China (973 Program) (2012CB932600, 2011CB911002), the National Natural Science Foundation of China (51222203, 51132006), a Juangsu Natural Science Fund for Distinguished Young Scholars (BK20130005), and a Project Funded by the Priority Academic Program Development (PAPD) of Jiangsu Higher Education Institutions.

Supporting Information Available: Additional characterization data, pharmacokinetics data, and results on MDR cancer cells. The Supporting Information is available free of charge on the ACS Publications website at DOI: 10.1021/acsnano.5b00640.

REFERENCES AND NOTES

1. Carney, D. N.; Mitchell, J. B.; Kinsella, T. J. *In Vitro* Radiation and Chemotherapy Sensitivity of Established Cell Lines of Human Small Cell Lung Cancer and Its Large Cell Morphological Variants. *Cancer Res.* **1983**, *43*, 2806–2811.
2. Donaldson, K. L.; Goolsby, G. L.; Wahl, A. F. Cytotoxicity of the Anticancer Agents Cisplatin and Taxol during Cell Proliferation and the Cell Cycle. *Int. J. Cancer* **1994**, *57*, 847–855.
3. Park, H.; Yang, J.; Lee, J.; Haam, S.; Choi, I.-H.; Yoo, K.-H. Multifunctional Nanoparticles for Combined Doxorubicin and Photothermal Treatments. *ACS Nano* **2009**, *3*, 2919–2926.
4. Peterson, C. M.; Lu, J. M.; Sun, Y.; Peterson, C. A.; Shiah, J.-G.; Straight, R. C.; Kopeček, J. Combination Chemotherapy and Photodynamic Therapy with N-(2-hydroxypropyl) Methacrylamide Copolymer-Bound Anticancer Drugs Inhibit Human Ovarian Carcinoma Heterotransplanted in Nude Mice. *Cancer Res.* **1996**, *56*, 3980–3985.
5. Gobin, A. M.; Lee, M. H.; Halas, N. J.; James, W. D.; Drezek, R. A.; West, J. L. Near-Infrared Resonant Nanoshells for Combined Optical Imaging and Photothermal Cancer Therapy. *Nano Lett.* **2007**, *7*, 1929–1934.
6. Hadziyannis, S. J.; Sette, H.; Morgan, T. R.; Balan, V.; Diago, M.; Marcellin, P.; Ramadori, G.; Bodenheimer, H.; Bernstein, D.; Rizzetto, M.; *et al*. Peginterferon-α2a and Ribavirin Combination Therapy in Chronic Hepatitis CA Randomized Study of Treatment Duration and Ribavirin Dose. *Ann. Int. Med.* **2004**, *140*, 346–355.
7. Zheng, M.; Yue, C.; Ma, Y.; Gong, P.; Zhao, P.; Zheng, C.; Sheng, Z.; Zhang, P.; Wang, Z.; Cai, L. Single-Step Assembly of DOX/ICG Loaded Lipid−Polymer Nanoparticles for Highly Effective Chemo-photothermal Combination Therapy. *ACS Nano* **2013**, *7*, 2056–2067.
8. Chen, Y.; Tan, C.; Zhang, H.; Wang, L. Two-Dimensional Graphene Analogues for Biomedical Applications. *Chem. Soc. Rev.* **2015**, 10.1039/C4CS00300D.
9. Lin, W.; He, C.; Liu, D. Self-Assembled Core-Shell Nanoparticles for Combined Chemotherapy and Photodynamic Therapy of Resistant Head and Neck Cancers. *ACS Nano* **2015**, *9*, 991–1003.
10. Wainwright, M. Photodynamic Antimicrobial Chemotherapy (PACT). *J. Antimicrob.Chemother.* **1998**, *42*, 13–28.
11. Zha, Z.; Yue, X.; Ren, Q.; Dai, Z. Uniform Polypyrrole Nanoparticles with High Photothermal Conversion Efficiency for Photothermal Ablation of Cancer Cells. *Adv. Mater.* **2013**, *25*, 777–782.
12. Jang, B.; Park, J.-Y.; Tung, C.-H.; Kim, I.-H.; Choi, Y. Gold Nanorod−Photosensitizer Complex for Near-Infrared Fluorescence Imaging and Photodynamic/Photothermal Therapy *in Vivo*. *ACS Nano* **2011**, *5*, 1086–1094.
13. Dong, K.; Liu, Z.; Li, Z.; Ren, J.; Qu, X. Hydrophobic Anticancer Drug Delivery by a 980 nm Laser-Driven Photothermal Vehicle for Efficient Synergistic Therapy of Cancer Cells *in Vivo*. *Adv. Mater.* **2013**, *25*, 4452–4458.
14. Chen, K.-J.; Chaung, E.-Y.; Wey, S.-P.; Lin, K.-J.; Cheng, F.; Lin, C.-C.; Liu, H.-L.; Tseng, H.-W.; Liu, C.-P.; Wei, M.-C.; *et al*. Hyperthermia-Mediated Local Drug Delivery by a Bubble-Generating Liposomal System for Tumor Specific Chemotherapy. *ACS Nano* **2014**, *8*, 5105–5115.
15. Cheng, L.; Wang, C.; Feng, L.; Yang, K.; Liu, Z. Functional Nanomaterials for Phototherapies of Cancer. *Chem. Rev.* **2014**, *114*, 10869–10939.
16. Fortin, J.-P.; Wilhelm, C.; Servais, J.; Ménager, C.; Bacri, J.-C.; Gazeau, F. Size-Sorted Anionic Iron Oxide Nanomagnets as Colloidal Mediators for Magnetic Hyperthermia. *J. Am. Chem. Soc.* **2007**, *129*, 2628–2635.
17. Devita, V. T.; Young, R. C.; Canellos, G. P. Combination *versus* Single Agent Chemotherapy: A Review of the Basis for Selection of Drug Treatment of Cancer. *Cancer* **1975**, *35*, 98–110.
18. Liu, T.; Wang, C.; Gu, X.; Gong, H.; Cheng, L.; Shi, X.; Feng, L.; Sun, B.; Liu, Z. Drug Delivery with PEGylated MoS_2 Nano-Sheets for Combined Photothermal and Chemotherapy of Cancer. *Adv. Mater.* **2014**, *26*, 3433–3440.
19. Gong, H.; Dong, Z.; Liu, Y.; Yin, S.; Cheng, L.; Xi, W.; Xiang, J.; Liu, K.; Li, Y.; Liu, Z. Engineering of Multifunctional Nano-Micelles for Combined Photothermal and Photodynamic Therapy under the Guidance of Multimodal Imaging. *Adv. Funct. Mater.* **2014**, *24*, 6492–6502.
20. Liu, J.; Wang, C.; Wang, X.; Wang, X.; Cheng, L.; Li, Y.; Liu, Z. Mesoporous Silica Coated Single-Walled Carbon Nanotubes as a Multifunctional Light-Responsive Platform for Cancer Combination Therapy. *Adv. Funct. Mater.* **2015**, *25*, 384–392.
21. Dai, Z.; Voigt, A.; Leporatti, S.; Donath, E.; Dähne, L.; Möhwald, H. Layer-by-Layer Self-Assembly of Polyelectrolyte and Low Molecular Weight Species into Capsules. *Adv. Mater.* **2001**, *13*, 1339–1342.
22. Ke, H.; Wang, J.; Dai, Z.; Jin, Y.; Qu, E.; Xing, Z.; Guo, C.; Yue, X.; Liu, J. Gold-Nanoshelled Microcapsules: A Theranostic Agent for Ultrasound Contrast Imaging and Photothermal Therapy. *J. Angew. Chem. Int. Ed.* **2011**, *123*, 3073–3077.
23. Song, G.; Wang, Q.; Wang, Y.; Lv, G.; Li, C.; Zou, R.; Chen, Z.; Qin, Z.; Huo, K.; Hu, R.; *et al*. Nanocomposites: A Low-Toxic Multifunctional Nanoplatform Based on Cu9S5@ $mSiO_2$ Core-Shell Nanocomposites: Combining Photothermal- and Chemotherapies with Infrared Thermal Imaging for Cancer Treatment. *Adv. Funct. Mater.* **2013**, *23*, 4280–4280.
24. Wang, N.; Zhao, Z.; Lv, Y.; Fan, H.; Bai, H.; Meng, H.; Long, Y.; Fu, T.; Zhang, X.; Tan, W. Gold Nanorod-Photosensitizer Conjugate with Extracellular pH-Driven Tumor Targeting Ability for Photothermal/Photodynamic Therapy. *Nano Res.* **2014**, *7*, 1291–1301.
25. Chen, Q.; Liang, C.; Wang, C.; Liu, Z. An Imagable and Photothermal "Abraxane-Like" Nanodrug for Combination Cancer Therapy to Treat Subcutaneous and Metastatic Breast Tumors. *Adv. Mater.* **2014**, *27*, 903–910.
26. Chen, Q.; Liang, C.; Wang, X.; He, J.; Li, Y.; Liu, Z. An Albumin-Based Theranostic Nano-Agent for Dual-Modal Imaging Guided Photothermal Therapy to Inhibit Lymphatic Metastasis of Cancer Post Surgery. *Biomaterials* **2014**, *35*, 9355–9362.
27. Chen, Q.; Wang, C.; Zhan, Z.; He, W.; Cheng, Z.; Li, Y.; Liu, Z. Near-Infrared Dye Bound Albumin with Separated Imaging and Therapy Wavelength Channels for Imaging-Guided Photothermal Therapy. *Biomaterials* **2014**, *35*, 8206–8214.
28. Céspedes, M. V.; Unzueta, U.; Tatkiewicz, W.; Sánchez-Chardi, A.; Conchillo-Solé, O.; Álamo, P.; Xu, Z.; Casanova, I.; Corchero, J. L.; Pesarrodona, M.; *et al*. *In Vivo* Architectonic Stability of Fully *de Novo* Designed Protein-Only Nanoparticles. *ACS Nano* **2014**, *8*, 4166–4176.
29. Weber, C.; Kreuter, J.; Langer, K. Desolvation Process and Surface Characteristics of HSA-Nanoparticles. *Int. J. Pharmaceut.* **2000**, *196*, 197–200.
30. Sheng, Z.; Hu, D.; Zheng, M.; Zhao, P.; Liu, H.; Gao, D.; Gong, P.; Gao, G.; Zhang, P.; Ma, Y.; *et al*. Smart Human Serum Albumin-Indocyanine Green Nanoparticles Generated by Programmed Assembly for Dual-Modal Imaging-Guided Cancer Synergistic Phototherapy. *ACS Nano* **2014**, *8*, 12310–12322.
31. Chen, S.-C.; Wu, Y.-C.; Mi, F.-L.; Lin, Y.-H.; Yu, L.-C.; Sung, H.-W. A Novel pH-Sensitive Hydrogel Composed of N, O-carboxymethyl Chitosan and Alginate Cross-Linked by Genipin for Protein Drug Delivery. *J. Controlled Release* **2004**, *96*, 285–300.
32. Lin, X.; Xie, J.; Niu, G.; Zhang, F.; Gao, H.; Yang, M.; Quan, Q.; Aronova, M. A.; Zhang, G.; Lee, S.; *et al*. Chimeric Ferritin Nanocages for Multiple Function Loading and Multimodal Imaging. *Nano Lett.* **2011**, *11*, 814–819.
33. Mertz, D.; Affolter-Zbaraszczuk, C.; Barthès, J.; Cui, J.; Caruso, F.; Baumert, T. F.; Voegel, J.-C.; Ogier, J.; Meyer, F. Templated Assembly of Albumin-Based Nanoparticles for Simultaneous Gene Silencing and Magnetic Resonance Imaging. *Nanoscale* **2014**, *6*, 11676–11680.
34. Mertz, D.; Wu, H.; Wong, J. S.; Cui, J.; Tan, P.; Alles, R.; Caruso, F. Ultrathin, Bioresponsive and Drug-Functionalized Protein Capsules. *J. Mater. Chem.* **2012**, *22*, 21434–21442.

35. Mertz, D.; Cui, J.; Yan, Y.; Devlin, G.; Chaubaroux, C.; Dochter, A.; Alles, R.; Lavalle, P.; Voegel, J. C.; Blencowe, A.; *et al*. Protein Capsules Assembled *via* Isobutyramide Grafts: Sequential Growth, Biofunctionalization, and Cellular Uptake. *ACS Nano* **2012**, *6*, 7584–7594.
36. Mertz, D.; Tan, P.; Wang, Y.; Goh, T. K.; Blencowe, A.; Caruso, F. Bromoisobutyramide as an Intermolecular Surface Binder for the Preparation of Free-Standing Biopolymer Assemblies. *Adv. Mater.* **2011**, *23*, 5668–5673.
37. Miele, E.; Spinelli, G. P.; Miele, E.; Tomao, F.; Tomao, S. Albumin-Bound Formulation of Paclitaxel (Abraxane® ABI-007) in the Treatment of Breast Cancer. *Int. J. Nanomed.* **2009**, *4*, 99.
38. Green, M.; Manikhas, G.; Orlov, S.; Afanasyev, B.; Makhson, A.; Bhar, P.; Hawkins, M. Abraxane®, a Novel Cremophor®-free, Albumin-Bound Particle form of Paclitaxel for the Treatment of Advanced Non-Small-Cell Lung Cancer. *Ann. Oncol.* **2006**, *17*, 1263–1268.
39. Xie, J.; Chen, K.; Lee, H.-Y.; Xu, C.; Hsu, A. R.; Peng, S.; Chen, X.; Sun, S. Ultrasmall c (RGDyK)-Coated Fe_3O_4 Nanoparticles and Their Specific Targeting to Integrin $\alpha v\beta 3$-Rich Tumor Cells. *J. Am. Chem. Soc.* **2008**, *130*, 7542–7543.
40. Lee, H.-Y.; Li, Z.; Chen, K.; Hsu, A. R.; Xu, C.; Xie, J.; Sun, S.; Chen, X. PET/MRI Dual-Modality Tumor Imaging Using Arginine-Glycine-Aspartic (RGD)−Conjugated Radiolabeled Iron Oxide Nanoparticles. *J. Nucl. Med.* **2008**, *49*, 1371–1379.
41. Zhen, Z.; Tang, W.; Chen, H.; Lin, X.; Todd, T.; Wang, G.; Cowger, T.; Chen, X.; Xie, J. RGD-Modified Apoferritin Nanoparticles for Efficient Drug Delivery to Tumors. *ACS Nano* **2013**, *7*, 4830–4837.
42. Zhu, Z.; Tang, Z.; Phillips, J. A.; Yang, R.; Wang, H.; Tan, W. Regulation of Singlet Oxygen Generation Using Single-Walled Carbon Nanotubes. *J. Am. Chem. Soc.* **2008**, *130*, 10856–10857.
43. Maiolo, J. R.; Ottinger, E. A.; Ferrer, M. Specific Redistribution of Cell-Penetrating Peptides from Endosomes to the Cytoplasm and Nucleus upon Laser Illumination. *J. Am. Chem. Soc.* **2004**, *126*, 15376–15377.
44. Kraft, S.; Diefenbach, B.; Mehta, R.; Jonczyk, A.; Luckenbach, G. A.; Goodman, S. L. Definition of an Unexpected Ligand Recognition Motif for $\alpha v\beta 6$ Integrin. *J. Biol. Chem.* **1999**, *274*, 1979–1985.
45. Munger, J. S.; Huang, X.; Kawakatsu, H.; Griffiths, M. J.; Dalton, S. L.; Wu, J.; Pittet, J.-F.; Kaminski, N.; Garat, C.; Matthay, M. A.; *et al*. The Integrin $\alpha v\beta 6$ Binds and Activates Latent TGFβ1: A Mechanism for Regulating Pulmonary Inflammation and Fibrosis. *Cell* **1999**, *96*, 319–328.
46. Williams, Ç. H.; Kajander, T.; Hyypiä, T.; Jackson, T.; Sheppard, D.; Stanway, G. Integrin $\alpha v\beta 6$ Is an RGD-Dependent Receptor for Coxsackievirus A9. *J. Virol.* **2004**, *78*, 6967–6973.
47. Bonnett, R. Photosensitizers of the Porphyrin and Phthalocyanine Series for Photodynamic Therapy. *Chem. Soc. Rev.* **1995**, *24*, 19–33.
48. MacDonald, T. D.; Liu, T. W.; Zheng, G. An MRI-Sensitive, Non-Photobleachable Porphysome Photothermal Agent. *Angew. Chem., Int. Ed.* **2014**, *126*, 7076–7079.
49. Caravan, P.; Ellison, J. J.; McMurry, T. J.; Lauffer, R. B. Gadolinium (III) Chelates as MRI Contrast Agents: Structure, Dynamics, and Applications. *Chem. Rev.* **1999**, *99*, 2293–2352.
50. Cheng, Z.; Thorek, D. L.; Tsourkas, A. Gadolinium-Conjugated Dendrimer Nanoclusters as a Tumor-Targeted T1Magnetic Resonance Imaging Contrast Agent. *Angew. Chem., Int. Ed.* **2010**, *49*, 346–350.
51. Bae, S.; Ma, K.; Kim, T. H.; Lee, E. S.; Oh, K. T.; Park, E.-S.; Lee, K. C.; Youn, Y. S. Doxorubicin-Loaded Human Serum Albumin Nanoparticles Surface-Modified with TNF-Related Apoptosis-Inducing Ligand and Transferrin for Targeting Multiple Tumor Types. *Biomaterials* **2012**, *33*, 1536–1546.
52. Li, Z.; Wang, C.; Cheng, L.; Gong, H.; Yin, S.; Gong, Q.; Li, Y.; Liu, Z. PEG-Functionalized Iron Oxide Nanoclusters Loaded with Chlorin e6 for Targeted, NIR Light Induced, Photodynamic Therapy. *Biomaterials* **2013**, *34*, 9160–9170.